11th World Congress on Computational Mechanics (WCCM XI)
5th European Conference on Computational Mechanics (ECCM V)
6th European Conference on Computational Fluid Dynamics (ECFD VI)
E. Oñate, J. Oliver and A. Huerta (Eds)

# FORM-FINDING OF INTERLACED SPACE STRUCTURES

**Seyed Sina Nabaei*, Olivier Baverel† AND Yves Weinand***

* Chaire of Timber Construction (IBOIS)
École Polytechnique Fédérale de Lausanne (EPFL)
CH-1015, Lausanne, Switzerland
e-mail: sina.nabaei@epfl.ch, web page: http://ibois.epfl.ch/ e-mail: yves.weinand@epfl.ch

†Navier research unit
École des Ponts ParisTech (ENPC)
Champes-Sur-Marne, France
e-mail: baverel@enpc.fr - Web page: http://navier.enpc.fr/

**Key words:** Space structures, Constrained nonlinear optimization, Discrete Elastic Rods

**Abstract.** By Interlaced Space Structures (ISS) we mean a coupled system of naturally curved flexible panels/strips interlaced together according to a design pattern. We are looking for a physically-based and efficient form-finding procedure in order to interactively explore different interlaced morphologies with respect to the design parameters for structural design purposes. Each panel is considered as an inextensible discrete kirchhoff rod and the rest shape of the coupled system rods is obtaibned via a constrained total energy minimization. The interlacing pattern is translated into a set of overlap order constraints and applied to the optimization problem. We employ an implementation of the interior-point filter linesearch algorithm with the Quasi-Newton procedure to solve the constrained nonlinear optimization and discuss the results through a case study.

## 1 INTRODUCTION

We are interested in a family of space structures where the geometry is behavior-based. It means that the curved shape of the structure is determined by the equilibrium of its flexible components deforming under the imposed loads and boundary conditions. The Euler Elastica rod [26, 23] is an example of such naturally curved configurations. Naturally curved structures are elastically resistant to external loads and deformations, offer a high structural performance, are large span and lightweight and are easy to erect. For all those reasons naturally curving has been a compelling form exploration process among the researchers working on the architectural geometry applications. [20] We focus the present study on Interlaced Space Structure (ISS), an actively curved structure composed of flexible linear structural components (strands) naturally curved from a flat initial state

and interlaced according to a design pattern. The concentration here has been on the case of ISS made by flexible strips (e.g. thin timber panels) without lack of generality.

### 1.1 Goals and contributions

We are looking for a physically-based quantitative (non-exact but efficient) form-finding tool in order to interactively explore interlaced morphologies for structural design purposes.

**Nonlinear static framework:** we formulate an offline constrained optimization problem based on the kinematics of Discrete Elastic Rod model (DER) [6] as a nonlinear static simulation. Since only the final rest shape matters for our design purpose, treating the problem in a static framework helps to surpass transition modes which would occur in a dynamic simulation. Moreover, Instead of iteratively solving for twists in a quasi-static step and then integrate for positions (as in [6]), we rather define positions and twists as variables of the optimization problem all at once.

**Interlace and inextensiblity constraints:** we use a Quasi-Newton procedure which only requires gradients and facilitates imposing various types of constraints on the system. Unlike the initial DER used for physically based animation, we do not need rigid body coupling features but complex strand-strand coupling constraints.

**A rich rod model for architectural geometry applications:** our implementation enhances the DER formulation for architectural geometry applications. We bring two main feature into the existing particle-based form-finding tools such as [29]: *(i)* the possibility to deal with general cross sections with proper elastic stiffness terms, instead of simplified spring stiffness which has to be interpreted each time and *(ii)* enhancing twist degrees of freedom which we believe can open the ground to discover twisted forms in actively curved complex structures.

### 1.2 Related work

Form finding of curved structures of all kinds has been the topic of several research publications. Tensioned structures [8, 4], tensegrity structures [33], gridshells [15, 2, 17], hybrid structures with coupled beams and membranes [14, 34] and actively curved thin shell structures [27, 21] are some examples of such curved complex structures among others. Each time simplified mechanics-based procedures have been proposed to deal with nonlinear equations of the form-finding problem with a focus on robustness and efficiency. The force density method [31] and its derived version trust network analysis [9], The surface stress density method [24], Dynamic Relaxation Method [3] and most recently the Particle based systems such as [29] are some of such developments approached in the community of architectural geometry research.

Elastic rods have been subject of intense ongoing research. Covered topics goes from computational mechanics [19, 13], DNA supercoiling Simulation [11, 32, 28] and robotics [30, 22] up to the physically based computer animation and virtual surgery simulators. [10,

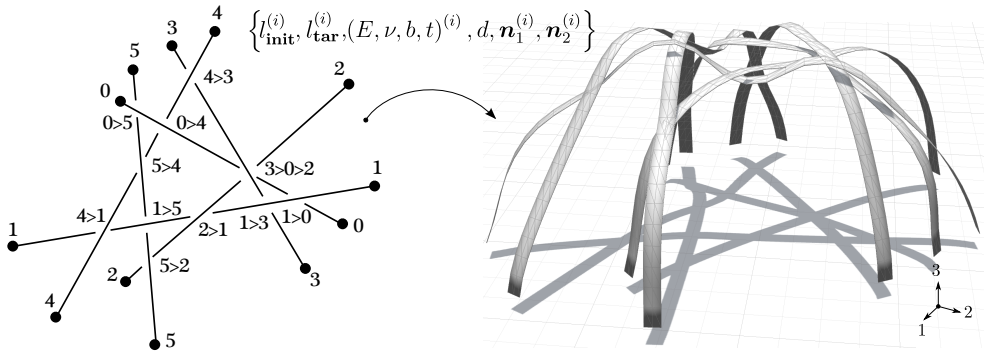


Figure 1: Graph representation of an ISS with its dual structure supposing the set of parameters $\left\{l^{(i)}_{\mathbf{init}}, l^{(i)}_{\mathbf{tar}}, (E,\nu,b,t)^{(i)}, d, \boldsymbol{n}^{(i)}_1, \boldsymbol{n}^{(i)}_2\right\}$ for each strand$^{(i)}$

25] Among existing models we have chosen the discrete Kirchhoff rod model introduced in the seminal research project carried out at Columbia Computer Graphics Group to study discrete geometric dynamics and artistic control of curves and surfaces. [5] The DER model has its origins heavily based on fast developing field of discrete differential geometry techniques. [16]

## 2 GEOMETRICAL FUNDAMENTALS

### 2.1 ISS graph representation

A graph representation is introduced in order to define and distinguish ISS morphologies. (see fig.1 left) Curves numbered at both ends represent strands and for intermediate nodes the relative overlap order of strands is noted using the $>$ notation. The graph representation enables to effectively sweep over interlaced configurations in an abstract topological form regardless of the dual 3D shape while there might be several of those duals corresponding to the same graph depending on panel's initial lengths and elastic properties and also the crossing's linking number.

### 2.2 Discrete Kirchhoff rod kinematics and elastic energies

**Notation:** For the sake of readability we follow the notation used in [6] in expressions, where vertex-based terms are noted with a subscript, edge-based quantities with a superscript and quantities referring to the initial state of the rod with an overline. While treating the system of coupled strands, an additional subscript will be used to distinguish quantities of separate strands.

The expressions for discrete bending and twist energies for a discrete kirchhoff rod with anisotropic cross section, flat initial state and zero initial twist are given in Eq.(1). These expressions are based on the curve-angle representation and the notion of the twist-free frame (so called Bishop frame). The concept has first appeared in [7] in its smooth form as an alternative to Frenet-Serret derivative based curve framing and recovered later in [6] for

the discrete representation. (see also [18] for detailed discussion and smooth energies) The main idea is heavily based on the notion of the parallel transport, interpreted for curves in $\mathbb{R}^3$. It is roughly to transport a quantity (here an adapted frame) along the tangent vector of the curve. In discrete framework a definition is required for the discrete parallel transport operator (and also its gradients) to be able to propagate the twist-free frame along the discrete curve edges as a reference to measure the material curvature. We adopt the same operator used in [6], which comes down to rotating the previous frame around the bi-normal vector to align $\boldsymbol{t}^{i-1}$ on $\boldsymbol{t}^{i}$. In order to equip a curve in $\mathbb{R}^3$ with twist-free frames, we have to start with an initial frame $\{\boldsymbol{t}^0, \boldsymbol{u}^0, \boldsymbol{v}^0\}$ and then parallel transport it along the curve edges. Notice that the first bishop frame coincides with the first material frame and that giving only $\boldsymbol{u}^0$ is enough to get the initial frame. We note this initial cross section orientation as $\boldsymbol{n}_1$ and take it as one of the parameter which have to be specified by the user. (see Fig.2 left) In energy expressions of Eq.1, $\boldsymbol{B}^j$ is the bending stiffness matrix for $j$th edge, $\beta$ is the torsional stiffness of the rod, $(\kappa \boldsymbol{b})_i$ the discrete curvature bi-normal and $\boldsymbol{\omega}$ is the discrete material curvature vector. For a rectangular cross section $b$ wide and $t$ thick, these stiffness quantities are noted in Eq. 3, some fundamental vector quantities are also illustrated in fig.2 and described in Eq. 2.

$$E_{bend}(\Gamma) = \sum_{i=1}^{n-1} \frac{1}{2\bar{l}_i} \Big( \sum_{j=i-1}^{i} (\boldsymbol{\omega}_i^j)^T \boldsymbol{B}^j \boldsymbol{\omega}_i^j \Big) \qquad E_{twist}(\Gamma) = \sum_{k=1}^{n-1} \frac{\beta \left(\theta^k - \theta^{k-1}\right)^2}{\bar{l}_k} \tag{1}$$

$$\boldsymbol{\omega}_i^j = \begin{pmatrix} \boldsymbol{m_2}^j \\ -\boldsymbol{m_1}^j \end{pmatrix} \cdot (\kappa \boldsymbol{b})_i : j \in \{i-1, i\} \qquad (\kappa \boldsymbol{b})_i = \frac{2\, \boldsymbol{e}^{i-1} \times \boldsymbol{e}^i}{\|\bar{\boldsymbol{e}}^{i-1}\| \, \|\bar{\boldsymbol{e}}^i\| + \boldsymbol{e}^{i-1} \cdot \boldsymbol{e}^i}$$
$$\begin{bmatrix} \boldsymbol{m_1}^j \\ \boldsymbol{m_2}^j \end{bmatrix} = \begin{bmatrix} cos\left(\theta^j\right) \boldsymbol{u}^j + sin\left(\theta^j\right) \boldsymbol{v}^j \\ -sin\left(\theta^j\right) \boldsymbol{u}^j + cos\left(\theta^j\right) \boldsymbol{v}^j \end{bmatrix} \qquad \bar{l}_i = \left(\bar{\boldsymbol{e}}^i \cdot \bar{\boldsymbol{e}}^i + \bar{\boldsymbol{e}}^{i-1} \cdot \bar{\boldsymbol{e}}^{i-1}\right)/2 \tag{2}$$

$$\boldsymbol{B} = \begin{pmatrix} \frac{th^3}{12} & 0 \\ 0 & \frac{ht^3}{12} \end{pmatrix}, \qquad \beta = \frac{Gwt^3}{3}, \qquad G = \frac{E}{2(1+\nu)} \tag{3}$$

## 3 OPTIMIZATION PROBLEM

We are looking for the final deformed state of the ISS and reformulate a static procedure replacing the dynamic integration proposed in [6]. We would not either apply the quasi-static material frame update as proceeded in [6], which also means that our energy gradient with respect to positions will be slightly different. Variables of the optimization problem are relaxed positions and material frame twist angles for all strands, assembled as a global vector of unknowns $\boldsymbol{u} = \left\{\theta^{(i)}, \boldsymbol{x}^{(i)}\right\}$. The values for energies, constraints, energy gradients and Jacobian of constraints are also global quantities containing contributions from all strands and the coupling constraints. Design parameters for each strand are position of end vertices $(\boldsymbol{x}_0^{(i)}, \boldsymbol{x}_n^{(i)})$, the initial length $(l_{\mathbf{init}}^{(i)})$ and targeted span $(l_{\mathbf{tar}}^{(i)})$, mechanical properties $(E, \nu, b, t)^{(i)}$, the panel offset to be respected at each overlap node $(d)$ and two

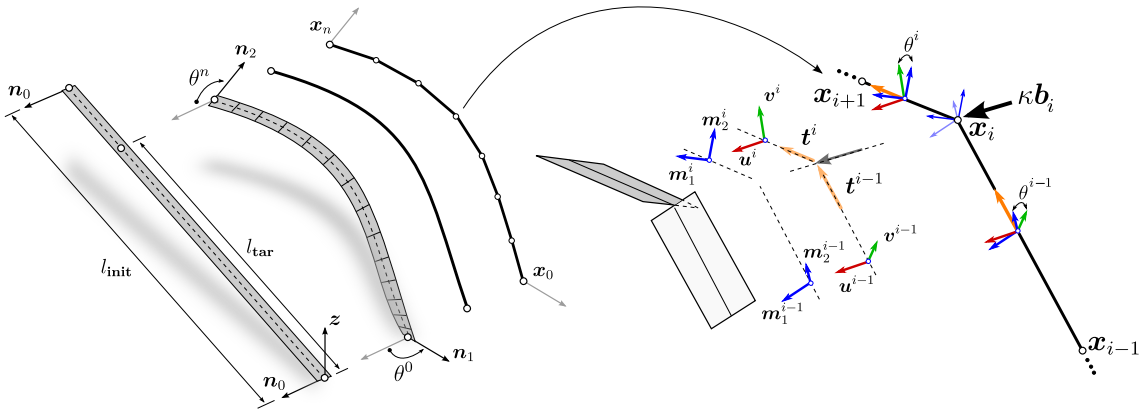


Figure 2: *left:* Design parameters and the discrete segmented representation. *right:* Angles and vectors used in the discrete notation. For $i$th edge: discrete Bishop frame $\{\boldsymbol{t}^i, \boldsymbol{u}^i, \boldsymbol{v}^i\}$, discrete material frame $\{\boldsymbol{t}^i, \boldsymbol{m}_1^i, \boldsymbol{m}_2^i\}$, twist angle $\theta^i$, tangent vector $\boldsymbol{t}^i$. For $i$th vertex discrete curvature binoraml vector is $\kappa \boldsymbol{b}_i$.

vectors indicating the cross section orientation to which start and end edges have to be aligned, respectively noted as $(\boldsymbol{n}_1^{(i)}, \boldsymbol{n}_2^{(i)})$. These design parameters are the input for our form-finding problem.

### 3.1 Formulation

We suppose the ISS is composed of a given number of strands defined by specifying the start and end vertices. We note $i$th strand as $\Gamma^{(i)}$. Instead of imposing all constraints at once to the flat initial state to get the interlaced - twisted - buckled configuration, we instead proceed with a three stage solution procedure formulated as constrained optimization problems detailed bellow.

**I. System of planar Elasticas of imposed total length and span** The initial optimization is to solve the inextensible Elastica problem. Strand$^{(i)}$ with initial length of $l_{\mathbf{init}}^{(i)}$ buckles to span $l_{\mathbf{tar}}^{(i)}$, with $n^{(i)}$ equal edges, fixed end vertices and under an additional constraint to keep the deformed configuration in the initial vertical plane. We note the normal to this plane as $\boldsymbol{n}_0^{(i)} = \boldsymbol{z} \times \boldsymbol{t}^{0(i)}$. This vector will also be used as the cross section orientation for first and last edges ($\theta^{0(i)} = \theta^{n(i)} = 0$) and to define the first Bishop frame as $\left\{\boldsymbol{t}^{0(i)}, \boldsymbol{n}_0^{(i)}, \boldsymbol{t}^{0(i)} \times \boldsymbol{n}_0^{(i)}\right\}$. The initial state for this first stage is the flat strand state. Each strand$^{(i)}$ with $n^{(i)}$ edges will contribute with respectively $(3(n^{(i)}-1)+n^{(i)}-2)$ and $(n^{(i)}+2)$ items to the assembled variables and constraints vector and the constraint Jacobian will have $(6(n^{(i)}-1)+6)$ extra non-zero items.

$$
\begin{aligned}
\min_{\{\theta^{(i)},\boldsymbol{x}^{(i)}\}} \quad & E(\theta,\boldsymbol{x}) = \sum_{(i)=0}^{\Gamma\ \text{count}} E_{bend}(\Gamma^{(i)}) + E_{twist}(\Gamma^{(i)}) \\
\text{s.t.} \quad & \textit{i)}\ \left\|\boldsymbol{x}_{j+1}^{(i)} - \boldsymbol{x}_{j}^{(i)}\right\|^2 = \left(l_{\mathbf{init}}^{(i)}\right)^2 / \left(n^{(i)}\right)^2 : \quad j \in \left\{0^{(i)}, \ldots, n^{(i)}-1\right\} \\
& \textit{ii)}\ \boldsymbol{x}_{j}^{(i)} = \bar{\boldsymbol{x}}_{j}^{(i)} \ : \quad j = 0^{(i)}, n^{(i)} \\
& \textit{iii)}\ \boldsymbol{n}_{0}^{(i)} \cdot \left(\boldsymbol{x}_{1}^{(i)} - \boldsymbol{x}_{0}^{(i)}\right) = 0 \\
& \textit{iv)}\ \boldsymbol{n}_{0}^{(i)} \cdot \left(\boldsymbol{x}_{n^{(i)}-1}^{(i)} - \boldsymbol{x}_{n^{(i)}}^{(i)}\right) = 0
\end{aligned}
$$

**II. System of twisted Elasticas:** as the next step we solve for the deformed system of twisted Elasticas and we suppose end edges to be clamped. The initial state for this analysis are deformed Elasticas retrieved by solving problem I described above. The cross section orientation at both ends for each strand are obtained by rotating the corresponding initial normal vector $\boldsymbol{n}_0^{(i)}$ respectively by $\theta^{0^{(i)}}$ and $\theta^{n(i)}$. (see Fig.2 left) Each strand$^{(i)}$ with $n^{(i)}$ edges will contribute with respectively $(3(n^{(i)}-3)+n^{(i)}-2)$ and $(n^{(i)}-2)$ items to the assembled variables and constraints vector and the constraint Jacobian will have $(6(n^{(i)}-1)+6)$ more non-zero items.

$$
\begin{aligned}
\min_{\{\theta^{(i)},\boldsymbol{x}^{(i)}\}} \quad & E(\theta,\boldsymbol{x}) = \sum_{(i)=0}^{\Gamma\ \text{count}} E_{bend}(\Gamma^{(i)}) + E_{twist}(\Gamma^{(i)}) \\
\text{s.t.} \quad & \textit{i)}\ \left\|\boldsymbol{x}_{j+1}^{(i)} - \boldsymbol{x}_{j}^{(i)}\right\|^2 = \left(l_{\mathbf{init}}^{(i)}\right)^2 / \left(n^{(i)}\right)^2 : \quad j \in \left\{1^{(i)}, \ldots, n^{(i)}-2\right\} \\
& \textit{ii)}\ \boldsymbol{x}_{j}^{(i)} = \bar{\boldsymbol{x}}_{j}^{(i)} \ : \quad j = 0^{(i)}, 1^{(i)}, n-1^{(i)}, n^{(i)} \\
& \textit{iii)}\ \text{Twist angle of material frames for first and last edges of strand}^{(i)} \\
& \quad \text{respectively } (\theta^0)^{(i)}, (\theta^{n^{(i)}-1})^{(i)} \text{aligned w.r.t } \boldsymbol{n}_1^{(i)} \text{ and } \boldsymbol{n}_2^{(i)}
\end{aligned}
$$

**III. Interlacing twisted Elasticas:** The final simulation step is dedicated to couple twisted strands according to the schematic interlace pattern. The initial state for this analysis is the result of problem II. For each overlap Strand$^{(i)}$ > Strand$^{(k)}$, a handle reference point is considered in 3D space to determine where exactly the overlap has to be passed. The vertices of the strands involved in the overlap (the ones closest to this handle point), noted as $\boldsymbol{x}_j^{(i)}$ and $\boldsymbol{x}_l^{(k)}$, will be the ones to hold the constraints. The distance between corresponding nodes of the overlapping strands, $\left\|\boldsymbol{x}_j^{(i)} - \boldsymbol{x}_l^{(k)}\right\|$, is set to be equal to the given offset distance $d$ and the top/bottom in the overlap is imposed using the projected distance of the involved nodes with respect to the material frame vector $\boldsymbol{m}_2^{(i)}$ of the strand$^{(i)}$. (The one which is passing on top) Each strand$^{(i)}$ with $n^{(i)}$ edges will contribute with respectively $(3(n^{(i)}-1)+n^{(i)}-2)$ and $(n^{(i)}-2)$ items to the assembled variables and constraints vector and the constraint Jacobian will have $(6(n^{(i)}-1)+6)$ more non-zero items. On top of that, for each overlap order of $(\boldsymbol{x}_j^{(i)} > \boldsymbol{x}_l^{(k)})$, 2 extra constraints have to be considered additionally and the constraint Jacobian will have $(4+3(n^{(i)}-3)+6)$ extra non-zero contribution to take into account the coupling.

$$
\begin{aligned}
\min_{\{\theta^{(i)},\boldsymbol{x}^{(i)}\}} \quad & E(\theta,\boldsymbol{x}) = \sum_{(i)=0}^{\Gamma\ \text{count}} E_{bend}(\Gamma^{(i)}) + E_{twist}(\Gamma^{(i)}) \\
\text{s.t.} \quad & \textit{i)}\ \left\|\boldsymbol{x}_{j+1}^{(i)} - \boldsymbol{x}_{j}^{(i)}\right\|^2 - \left(l_{\mathbf{init}}^{(i)}/n^{(i)}\right)^2 = 0: \quad j \in \left\{1^{(i)},\ldots,n^{(i)}-2\right\} \\
& \textit{ii)}\ \boldsymbol{x}_{j}^{(i)} - \bar{\boldsymbol{x}}_{j}^{(i)} = 0 \ : \quad j = 0^{(i)}, 1^{(i)}, n-1^{(i)}, n^{(i)} \\
& \textit{iii)}\ \text{Twist angle of material frames for first and last edges of strand}^{(i)} \\
& \quad \text{respectively } (\theta^0)^{(i)}, (\theta^{n^{(i)}-1})^{(i)} \text{aligned w.r.t } \boldsymbol{n}_1^{(i)} \text{ and } \boldsymbol{n}_2^{(i)} \\
& \textit{iv)}\ \textbf{foreach}\ \left(\boldsymbol{x}_{j}^{(i)} > \boldsymbol{x}_{l}^{(k)} \text{order constraint}\right) \\
& \quad \left\|\boldsymbol{x}_{j}^{(i)} - \boldsymbol{x}_{l}^{(k)}\right\|^2 - d^2 = 0 \qquad \text{(see 3.3)} \\
& \quad \left(\boldsymbol{x}_{j}^{(i)} - \boldsymbol{x}_{l}^{(k)}\right) \cdot (\boldsymbol{m}_2^j)^{(i)} - d = 0 \qquad \text{(see 3.3)}
\end{aligned}
$$

We proceed to solve the above cited problems using a Quasi-Newton procedure with BFGS approximation of the Hessians using IPOPT [35] as the optimization core and HSL solver Ma27.[1] IPOPT is an open source implementation of a primal-dual interior-point algorithm with a filter line-search method for nonlinear programming. We need analytical expressions for the gradients of energies and constraints for this purpose discussed in following lines.

### 3.2 Energy gradients

The expressions for energy gradients are mainly recalled from [6]. For the sake of simplicity, equations are discussed for a single strand suppressing the strand superscripts. Contributions from all strands are assembled in a global vector of energy gradient $\nabla e$ which is evaluated along with the objective function of total energy by the optimization core at each iteration.

The expression for energy derivatives with respect to $\theta^j$ are needed for all intermediate nodes. Twist energy depends explicitly on twist angles whereas the bending energy is related to twist mainly through the material curvatures vector. While vertex positions remain unchanged with respect to variation of $\theta^j$, bi-normal curvature $(\kappa \boldsymbol{b})_i$ and Bishop frames $\{\boldsymbol{t}^j, \boldsymbol{u}^j, \boldsymbol{v}^j\}$ will not contribute and this also means that the partial and total derivatives with respect to $\theta^j$ are equivalent. The expression for $\frac{\mathrm{d}E(\Gamma)}{\mathrm{d}\theta^j}$ follows, where $\boldsymbol{J} = \left(\begin{smallmatrix} 0 & -1 \\ 1 & 0 \end{smallmatrix}\right)$ operates as a counterclockwise rotation of $\frac{\pi}{2}$ around the edge tangent vector.

$$
\frac{\mathrm{d}E(\Gamma)}{\mathrm{d}\theta^j} = \frac{1}{\bar{l}_j}\left(\boldsymbol{\omega}_j^j\right)^T \boldsymbol{J}\boldsymbol{B}^j\boldsymbol{\omega}_j^j + \frac{1}{\bar{l}_{j+1}}\left(\boldsymbol{\omega}_{j+1}^j\right)^T \boldsymbol{J}\boldsymbol{B}^j\boldsymbol{\omega}_{j+1}^j + \frac{2\beta\left(\theta^j - \theta^{j-1}\right)}{\bar{l}_j} - \frac{2\beta\left(\theta^{j+1} - \theta^j\right)}{\bar{l}_{j+1}} \tag{4}
$$

In terms of Energy gradients with respect to $\boldsymbol{x}_i$, variation of centerline position will modify how discrete Bishop frame travels along the discrete curve, so two contribution appear from terms depending on position degrees of freedom and the terms coupling twist angles to positions.

$$\frac{\mathrm{d}E(\Gamma)}{\mathrm{d}\boldsymbol{x}_i} = \sum_{k=1}^{n-1} \frac{1}{\bar{l}_k} \Big( \sum_{j=k-1}^{k} \Big(\nabla_i \boldsymbol{\omega}_k^j\Big)^T \boldsymbol{B}^j \boldsymbol{\omega}_k^j \Big) + \sum_{j=1}^{n-1} \left(E(\Gamma)_{,\theta^j} \, \nabla_i \theta^j\right) \tag{5}$$

Notice that twist energy does not depend explicitly on $\boldsymbol{x}$ and is excluded from the first gradient expression. The material curvature derivative is given by:

$$\nabla_i \boldsymbol{\omega}_k^j = \begin{bmatrix} \boldsymbol{m_2}^j \\ -\boldsymbol{m_1}^j \end{bmatrix} \cdot \nabla_i \left(\kappa \boldsymbol{b}\right)_k - \boldsymbol{J}\boldsymbol{\omega}_k^j \otimes \nabla_i \theta^j \tag{6}$$

The $(\kappa \boldsymbol{b})_k$ is a function of $\boldsymbol{x}_{k-1}$, $\boldsymbol{x}_k$ and $\boldsymbol{e}^{k+1}$. The non-zero terms for $\nabla_i \left(\kappa \boldsymbol{b}\right)_k$ can be summarized as follows. $[\boldsymbol{u}]_\times$ is the cross product matrix of vector $\boldsymbol{u}$ with $\boldsymbol{\mathcal{E}} = \varepsilon_{ijk} \boldsymbol{e}_i \otimes \boldsymbol{e}_j \otimes \boldsymbol{e}_k$ being the permutation tensor of order three.

$$\begin{cases} \nabla_{k-1} \ (\kappa \boldsymbol{b})_k & = \frac{2\left[\boldsymbol{e}^k\right]_\times + \boldsymbol{e}^k \otimes (\kappa \boldsymbol{b})_k}{\alpha} \\ \nabla_{k+1} \ (\kappa \boldsymbol{b})_k & = \frac{2\left[\boldsymbol{e}^{k-1}\right]_\times - \boldsymbol{e}^{k-1} \otimes (\kappa \boldsymbol{b})_k}{\alpha} \\ \nabla_{k} \ (\kappa \boldsymbol{b})_k & = -\left(\nabla_{k-1} + \nabla_{k+1}\right) \ (\kappa \boldsymbol{b})_k \end{cases}, \qquad \begin{cases} \alpha & = \left\|\bar{\boldsymbol{e}}^{k-1}\right\| \left\|\bar{\boldsymbol{e}}^{k}\right\| + \boldsymbol{e}^{k-1} \cdot \boldsymbol{e}^k \\ [\boldsymbol{u}]_\times & = -\boldsymbol{\mathcal{E}} \cdot \boldsymbol{u} \end{cases} \tag{7}$$

The variation of the twist angle with respect to vertex position variation is also given as $\nabla_i \theta^j = \sum_{k=1}^{j} \nabla_i \psi_k$ which comes form the notion of discrete Holonomy of the parallel transport connection for discrete curves in $\mathbb{R}^3$. [6, 12] The variation of discrete Holonomy will give us how much an adapted frame will be extra twisted, while parallel transported along a discrete curve with respect to variation of its vertices which is the ingredient we are looking for. The non-zero contributions of $\nabla_i \psi_k$ are:

$$\begin{cases} \nabla_{k-1} \, \psi_k & = \frac{(\kappa \boldsymbol{b})_k}{2\|\boldsymbol{e}^{k-1}\|} \\ \nabla_{k} \, \psi_k & = -\left(\nabla_{k-1} + \nabla_{k+1}\right) \, \psi_k \\ \nabla_{k+1} \, \psi_k & = -\frac{(\kappa \boldsymbol{b})_k}{2\|\boldsymbol{e}^{k}\|} \end{cases} \tag{8}$$

### 3.3 Gradient of constraints

For each optimization problem, constraints are assembled in a global vector of $\boldsymbol{c}$. Here the elements of $\nabla \boldsymbol{c}$ are provided for the main employed constraints: the edge length or inextensibility constraints, overlap order constraints and the constraints used to keep an edge normal to the strand initial plane. The interface with the optimization core is proceed with a sparse Jacobian construction, so only the non-zero items and their global index will be transmitted. The segment length for $j$th edge is imposed as an equality constraint with respect to its vertex coordinates as $m_l = \|\boldsymbol{x}_{j+1} - \boldsymbol{x}_j\|^2 - (l_{\mathbf{init}}/n)^2 = 0$. The nonzero derivatives are $\nabla_j \, m_l = -\left(\boldsymbol{x}_{j+1} - \boldsymbol{x}_j\right)$ and $\nabla_{j+1} \, m_l = \left(\boldsymbol{x}_{j+1} - \boldsymbol{x}_j\right)$. The constraint for keeping the offset between the overlap nodes in optimization problem III is imposed similarly.

The constraint used to impose the overlap order ($\boldsymbol{x}_j^{(i)} > \boldsymbol{x}_l^{(k)}$) is formulated with respect to the material frame vector of the top strand $(\boldsymbol{m}_2^j)^{(i)}$ as $m_o = \left(\boldsymbol{x}_j^{(i)} - \boldsymbol{x}_l^{(k)}\right) \cdot (\boldsymbol{m}_2^j)^{(i)} - d = 0$. The non-zero contributions to the assembled constraint Jacobian appear while computing gradients with respect to $\boldsymbol{x}_j^{(i)}$, $\boldsymbol{x}_l^{(k)}$ and $\theta^{j(i)}$ as follows.

$$\begin{cases} \frac{\partial m_o}{\partial \boldsymbol{x}_j^{(i)}} & = (\boldsymbol{m}_2^j)^{(i)} - \left(\boldsymbol{x}_j^{(i)} - \boldsymbol{x}_l^{(k)}\right) \cdot (\boldsymbol{m}_1^j)^{(i)} \otimes \frac{\partial \theta^{j\,(i)}}{\partial \boldsymbol{x}_j^{(i)}} \\ \frac{\partial m_o}{\partial \boldsymbol{x}_l^{(k)}} & = -(\boldsymbol{m}_2^j)^{(i)} \\ \frac{\partial m_o}{\partial \theta^{j\,(i)}} & = -\left(\boldsymbol{x}_j^{(i)} - \boldsymbol{x}_l^{(k)}\right) \cdot (\boldsymbol{m}_1^j)^{(i)} \end{cases} \tag{9}$$

Constraints to keep an edge laid in the plan specified by the normal vector $\boldsymbol{n}_0$ are used in optimization problem I (see 3.1) and are formulated as $m_p = \boldsymbol{n}_0^{(i)} \cdot (\boldsymbol{x}_1^{(i)} - \boldsymbol{x}_0^{(i)}) = 0$. Two non-zero contribution of such constraint into the assembled constraint Jacobian are $\frac{\partial m_p}{\partial \boldsymbol{x}_0^{(i)}} = -\boldsymbol{n}_0^{(i)}$ and $\frac{\partial m_p}{\partial \boldsymbol{x}_1^{(i)}} = \boldsymbol{n}_0^{(i)}$.

## 4 CASE STUDY

We approach with a simple case study to show the relationship between the 2D graph representation and its dual ISS variants with respect to two main parameters: the position of the overlap handle point and overlap order variation. The simple ISS shown in fig. 3 (right) is consisted of three panels interlaced at a single intermediate point with the following design parameters. Elastic properties are identical for all panels chosen to represent mean wood elastic constants $E = 8000$ Mpa, $\nu = 0.3$, $b = 150\,mm$, $t = 6\,mm$, overlap offset $d = 200\,mm$, initial lengths $l_{\mathbf{init}}^{(i)}$ are $\{6.0\,m, 5.5\,m, 7.5\,m\}$ and targeted span lengths $l_{\mathbf{tar}}^{(i)}$ are $\{3.9\,m, 4.0\,m, 5.1\,m\}$. Cross section orientations are illustrated in fig. 3 and identical twist of $45\,^\circ$ is applied on the end vertex of all three panels, each of them equally segmented to 21 edges. In order to see how position of handle point can modify the 3D dual shape of the ISS, two variants are generated by only changing the handle point, highlighted in fig. 3. Furthermore keeping the handle point at the same position of variant1 in fig. 3, the overlap order of panel is changed to generate possible overlaps of three panels over the intermediate point illustrated in fig. 4.

More complex ISS morphologies are not far from reach like the structure illustrated in fig. 1 (right) involving several strands with more populated overlaps.

## 5 CONCLUSION AND FUTURE WORK

We introduced a new form-finding procedure to deal with naturally curved interlaced structures by approaching the nonlinear equilibrium of the coupled system as a constrained optimization problem. We enhance the research community working on actively bent structures with an implementation of a rich rod model with two main capabilities of capturing twist degrees of freedom and handling anisotropic cross sections. We believe this tool can open perspectives to a new generation of actively curved girdshell-like struc-

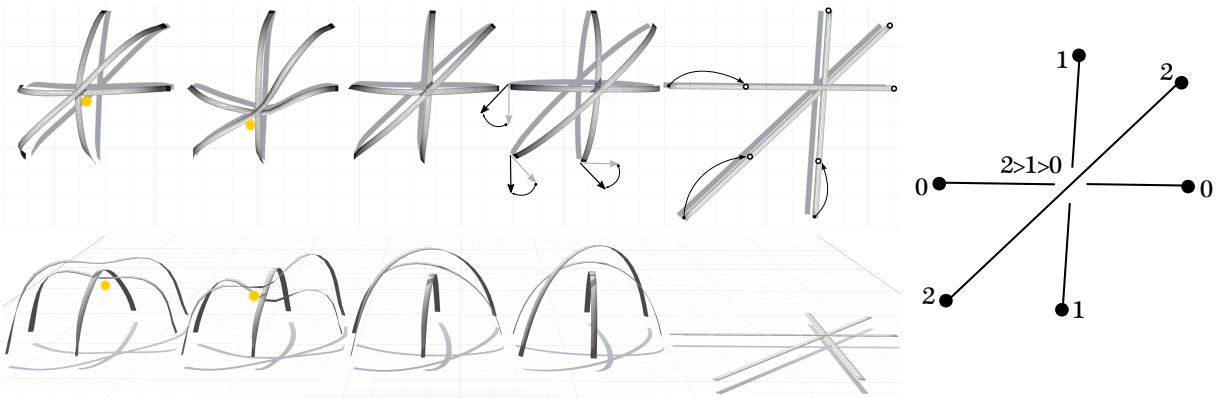


Figure 3: *right to left:* ISS graph representation, flat initial state, system of Elasticas, System of twisted Elasticas, interlaced Variant1, interlaced Variant2.

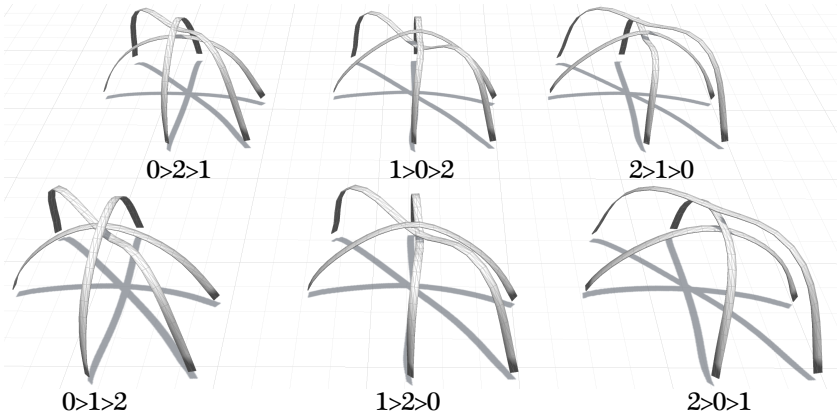


Figure 4: ISS variants with respect to the overlap order

tures made with panels and also empowers the research on actively twisted structures with complex geometry such as twisted gridshells. We segmented the simulation pipeline as three optimization problems: form-finding of Elastica, the twisted Elastica and the coupled system of twisted Elastica. Whereas our focus has been to solve the coupled problem, we also believe that the first two form-finding procedures on their own can raise a lot of interest among the community of researchers and students working on actively curved structures. Two main complementary studies remaining to approach in a futures publication on the topic are: built prototypes and comparison for some complex ISS generated by the tool and enhancing constraints to couple strands on their end vertices as well, provided that the present study enables only intermediate coupling.

## 6 ACKNOWLEDGMENT

This work was sponsored by the Swiss National Science Foundation (SNSF) under grant No. 200021_137884/1. This support is gratefully acknowledged. Authors would

like also to thank Basile Audoly and Eitan Grinspun for their constructive remarks on problem formulation and implementation.

## REFERENCES

[1] Hsl(2013). a collection of fortran codes for large scale scientific computation. http://www.hsl.rl.ac.uk.

[2] Adriaenssens, S., and Barnes, M. Tensegrity spline beam and grid shell structures. *Engineering structures 23*, 1 (2001), 29–36.

[3] Barnes, M. Form-finding and analysis of prestressed nets and membranes. *Computers & Structures 30*, 3 (1988), 685–695.

[4] Barnes, M. R. Form finding and analysis of tension structures by dynamic relaxation. *International journal of space structures 14*, 2 (1999), 89–104.

[5] Bergou, M., and Adviser-Grinspun, E. *Discrete geometric dynamics and artistic control of curves and surfaces*. Columbia University, 2010.

[6] Bergou, M., Wardetzky, M., Robinson, S., Audoly, B., and Grinspun, E. Discrete elastic rods. *ACM Transactions on Graphics (TOG) 27*, 3 (2008), 63.

[7] Bishop, R. L. There is more than one way to frame a curve. *American Mathematical Monthly* (1975), 246–251.

[8] Bletzinger, K.-U., Wüchner, R., Daoud, F., and Camprubí, N. Computational methods for form finding and optimization of shells and membranes. *Computer Methods in Applied Mechanics and Engineering 194*, 30 (2005), 3438–3452.

[9] Block, P., and Ochsendorf, J. Thrust network analysis: a new methodology for three-dimensional equilibrium. *journal of IASS 155* (2007), 167.

[10] Chentanez, N., Alterovitz, R., Ritchie, D., Cho, L., Hauser, K. K., Goldberg, K., Shewchuk, J. R., and O'Brien, J. F. *Interactive simulation of surgical needle insertion and steering*, vol. 28. ACM, 2009.

[11] Clauvelin, N., Audoly, B., and Neukirch, S. Mechanical response of plectonemic dna: An analytical solution. *Macromolecules 41*, 12 (2008), 4479–4483.

[12] de Vries, R. Evaluating changes of writhe in computer simulations of supercoiled dna. *The Journal of chemical physics 122*, 6 (2005), 064905.

[13] Dias, M. A., and Audoly, B. A non-linear rod model for folded elastic strips. *Journal of the Mechanics and Physics of Solids 62* (2014), 57–80.

[14] Dieringer, F., Philipp, B., Wüchner, R., and Bletzinger, K.-U. Numerical methods for the design and analysis of hybrid structures. *International Journal of Space Structures 28*, 3 (2013), 149–160.

[15] Douthe, C., Baverel, O., and Caron, J.-F. Form-finding of a grid shell in composite materials. *Journal-International association for shell and Spatial Structures 150* (2006), 53.

[16] Grinspun, E., Schröder, P., and Desbrun, M. Discrete differential geometry: an applied introduction. *ACM SIGGRAPH Course 7* (2006).

[17] Hernández, E. L., Gengnagel, C., Sechelmann, S., and Rörig, T. On the materiality and structural behaviour of highly-elastic gridshell structures. In *Computational Design Modelling*. Springer, 2012, pp. 123–135.

[18] Langer, J., and Singer, D. A. Lagrangian aspects of the kirchhoff elastic rod. *SIAM review 38*, 4 (1996), 605–618.

[19] Lazarus, A., Miller, J., and Reis, P. Continuation of equilibria and stability of slender elastic rods using an asymptotic numerical method. *Journal of the Mechanics and Physics of Solids 61*, 8 (2013), 1712–1736.

[20] Lienhard, J., Alpermann, H., Gengnagel, C., and Knippers, J. Active bending, a review on structures where bending is used as a self-formation process. *International Journal of Space Structures 28*, 3 (2013), 187–196.

[21] Lienhard, J., Schleicher, S., Poppinga, S., Masselter, T., Milwich, M., Speck, T., and Knippers, J. Flectofin: a hingeless flapping mechanism inspired by nature. *Bioinspiration & biomimetics 6*, 4 (2011), 045001.

[22] Lock, J., Laing, G., Mahvash, M., and Dupont, P. E. Quasistatic modeling of concentric tube robots with external loads. In *Intelligent Robots and Systems (IROS), 2010 IEEE/RSJ International Conference on* (2010), IEEE, pp. 2325–2332.

[23] Love, A. E. H. *A treatise on the mathematical theory of elasticity*. Cambridge University Press, 2013.

[24] Maurin, B., and Motro, R. The surface stress density method as a form-finding tool for tensile membranes. *Engineering structures 20*, 8 (1998), 712–719.

[25] Miller, J., Lazarus, A., Audoly, B., and Reis, P. Shapes of a suspended curly hair. *Physical review letters 112*, 6 (2014), 068103.

[26] Mumford, D. *Elastica and computer vision*. Springer, 1994.

[27] Nabaei, S. S., Baverel, O., and Weinand, Y. Mechanical form-finding of the timber fabric structures with dynamic relaxation method. *International Journal of Space Structures 28*, 3 (2013), 197–214.

[28] Olson, S. D., Lim, S., and Cortez, R. Modeling the dynamics of an elastic rod with intrinsic curvature and twist using a regularized stokes formulation. *Journal of Computational Physics 238* (2013), 169–187.

[29] Piker, D. Kangaroo: Form finding with computational physics. *Architectural Design 83*, 2 (2013), 136–137.

[30] Rucker, D. C., Webster, R. J., Chirikjian, G. S., and Cowan, N. J. Equilibrium conformations of concentric-tube continuum robots. *The International Journal of Robotics Research 29*, 10 (2010), 1263–1280.

[31] Schek, H.-J. The force density method for form finding and computation of general networks. *Computer methods in applied mechanics and engineering 3*, 1 (1974), 115–134.

[32] Shi, Y., and Hearst, J. E. The kirchhoff elastic rod, the nonlinear schrödinger equation, and dna supercoiling. *The Journal of chemical physics 101*, 6 (1994), 5186–5200.

[33] Tibert, A., and Pellegrino, S. Review of form-finding methods for tensegrity structures. *International Journal of Space Structures 18*, 4 (2003), 209–223.

[34] Van Mele, T., De Laet, L., Veenendaal, D., Mollaert, M., and Block, P. Shaping tension structures with actively bent linear elements. *International Journal of Space Structures 28*, 3 (2013), 127–136.

[35] Wächter, A., and Biegler, L. T. On the implementation of an interior-point filter line-search algorithm for large-scale nonlinear programming. *Mathematical programming 106*, 1 (2006), 25–57.